Porous Carbon doped by different nitrogen sources and its Electrochemical Properties

Mengqi Du[1], Yanshuang Meng[1], Lei Wang[1], Chaoyu Duan[1],
Fuliang Zhu[1,3,] and Yue Zhang[2,*]*

[1] School of Materials Science and Engineering, Lanzhou University of Technology, Lanzhou 730050,China
[2] Department of Mechanical and Industrial Engineering, Texas A&M University-Kingsville, Kingsville, Texas, 78363, USA
[3] State Key Laboratory of Advanced Processing and Recycling of Non-ferrous Metals, Lanzhou 730050, China
[*]E-mail: chzfl@126.com (Fuliang Zhu), yue.zhang@tamuk.edu (Yue Zhang)

Nitrogen doped porous carbons (NPCs) were synthesized by using a self-sacrificing template method. The obtained NPCs exhibit large amount of mesopores and high pyrrolic N and pyridine N content. Because the pyrrolic N and pyridine N facilitate the formation of defects and vacancies, the electrochemical properties of NPCs are significantly improved. The NPCs delivers a high reversible capacity of 621 mAh g^{-1} at 0.1 C after 50 cycles and excellent rate capacity of 456 mAh g^{-1} at 1 C, showing great potentials as anode materials for Li-ion batteries (LIBs).

1. INTRODUCTION

In recent decades, LIBs are widely used in power transport, portable electronic equipment, electric vehicles and other electric tools due to their long cycle life and high energy density [1-5]. However, graphite, as carbon traditional anode materials, has been unable to meet the high performance requirements of LIBs because of its low specific capacity (372mAh g^{-1}), poor cycle life and rate performance [6-8]. In order to solve these problems, porous carbon has been the focus of researches in recent years due to its unique structure and physical performance [9-12]. High specific surface area of porous carbon can provide a large number of active sites and a large amount of mesopores, which shorten the diffusion distance of Li^+ in porous carbon networks[13, 14]. Therefore,

porous carbon with reasonable pore size distribution and pore structure exhibits excellent cycle performance and rate performance.

It is well known that nitrogen-doping is an effective way to improve the electrochemical properties of porous carbon [15-18]. Because of the strong electronic conductivity of nitrogen, nitrogen doping can not only modify the electronic conductivity of porous carbon, but also introduce a large number of defects and vacancies, thereby increasing the active sites of carbon materials and the wettability of the electrode/electrolyte [19, 20]. Furthermore, previous reports have suggested that nitrogen doping can increase the electron density of the Fermi level and improve the stability of nitrogen doped porous carbons [21, 22]. However, when nitrogen-doped porous carbons are used as anode materials for LIBs, not all nitrogen-doped atoms play a beneficial role in the reversible capacity of porous carbon materials. For example, Wang and his co-worker reported that graphitic N could significantly increase the energy of the carbon framework, while the nitrogen doped carbon exhibited poor cycling performance due to its low structure stability during the charge-discharge cycles [23]. Tian and her co-worker suggested that graphitic N had the lowest lithium storage capacity compared to pyrrolic N and pyridine N by calculating the average absorption energy of Li^+ in three nitrogen-doping structural models using first principles[24]. In addition, Yang group and Guo group proposed that due to the high electrochemical activity of pyridinic N or pyrrolic N with sp^2 carbon, a high density state of the ð electron delocalization is beneficial to the adsorption behavior of Li^+ and capacitance [25, 26]. Therefore, it is critical to understand the key factors that affect the formation of different types of nitrogen and to synthesize NPCs with low graphite N content.

In this work, NPCs with high pyrrolic N and pyridine N content were produced by using self-sacrifice template method. The effect of nitrogen type and specific surface area on the electrochemical performance of the NPCs was investigated. It was found that a higher specific surface led to a lower content of graphitic N, which could improve the electrochemical performance of NPCs..

2. EXPERIMENTAL

2.1 Synthesis of polyethylene (PS) template and poly acrylonitrile (PAN)

The PS template was synthesized by soap-free emulsion method. In a typical experiment, 0.026 g dodecyl sulfate and 0.075 g $NaHCO_3$ were dissolved in 150 ml deionized water. After stirring at 70 ^{o}C for 20 min, 15 g styrene was added to the solution and stirred for another 10 min. Then, 0.34 g $K_2S_2O_8$ was added as an initiator to the mixture and stirred at 70 ^{o}C under an argon atmosphere for 10 h. Finally, the white product was collected after washing with ethanol and deionized water and drying at 80 ^{o}C for 24 h.

To syntheize the PAN, 15 g acrylonitrile was dissolved in 150 ml deionized water and stirred at 60 ^{o}C for 20 min. Then 0.02 g $K_2S_2O_8$ was added as an initiator to the mixture and stirred at 60 ^{o}C under an argon atmosphere for 8 h. The PAN was washed and dried in the same way as the PS template.

2.2 Synthesis of NPCs and NCMSs

The NPCs was synthesized by using 1 g PS template and 3 g PAN. A control sample were prepared by using 3 g PAN solely and denoted as nitrogen doped carbon materials (NCMs). In pre-oxidation stage, both samples were heated to 280 ^{o}C at a ramp rate of 1 ^{o}C·min^{-1} in an air flow for 1 h. In the carbonization stage, the samples were carbonized at 900 ^{o}C under argon atmosphere for 1 h with a ramp rate of 5 ^{o}C·min^{-1}.

2.3 Structure and morphology characterization

The morphologies of NPCs and NCMs were observed on field emission scanning electron microscope (FESEM, JSM-6701F,Japan electronics optics co.,ltd , Japan) under the acceleration voltage of 20 kV. X-ray photoelectron spectroscopy (XPS, ESCALAB 250Xi, Thermo Fisher Scientific.) was recorded. Raman spectra of the samples were recorded on LabRAM HR UV/vis/NIR (Honba Jobin Yvon, France). Nitrogen adsorption and desorption isotherms was performed on ASAP 2020 (Micromeritics Instrument Crop, America). The surface area and pore size distribution were calculated by using BET and DJH methods, respectively. The total pore volume was calculated by the adsorption amount of nitrogen at relative pressure(P/P$_0$) of 0.99.

2.4 Electronchemical characterization

CR2032 coin-type test cell was assembled to characterize the electrochemical properties of the samples as anode materials. The working electrode was prepared by a slurry of the prepared materials (80 wt%), polyvinylidenefluoride (PVDF, 10wt%), and acetylene black (10wt%) in N-methyl-2-pyrrolidone (NMP). The slurry was coated onto a Cu film and dried in vacuum at 80 ºC for 12 h. For the preparation of electrolyte solution, 1 M LiPF$_6$ was dissolved in a mixture of ethylene carbonate (EC) and 1,2-dimethoxyethane (DMC) with a volume ratio of 1:1. The Li foil and the Celgard membrane (Celgard 2400) were used as counter electrode separator, respectively. The cell was tested after standing for 24 hours. The galvanostatic charge-discharge cycle was measure with LAND CT2001A test system at room temperature. Cycle voltammetry (CV) curves were recorded between the voltage range of 0.005 V to 3.0 V at a scanning rate of 0.1 mV s^{-1} on the CHI 660D electrochemical workstation. The electrochemical impedance spectroscopy (EIS) was carried out on the same equipment within the frequency from 0.01 Hz to 10^5 Hz.

3. RESULTS AND DISCUSSION

Figure 1 shows the SEM images of NCMs and NPCs. Compared with NCMs, NPCs exhibit a rougher surface with many mesopores and macropores of different size. This difference between NCMs and NPCs is due to the addition of PS templates during the preparation process. The relatively

poor miscibility between PS templates and PAN was the main reason for formation of mesopores and macopores in NPCs [27].
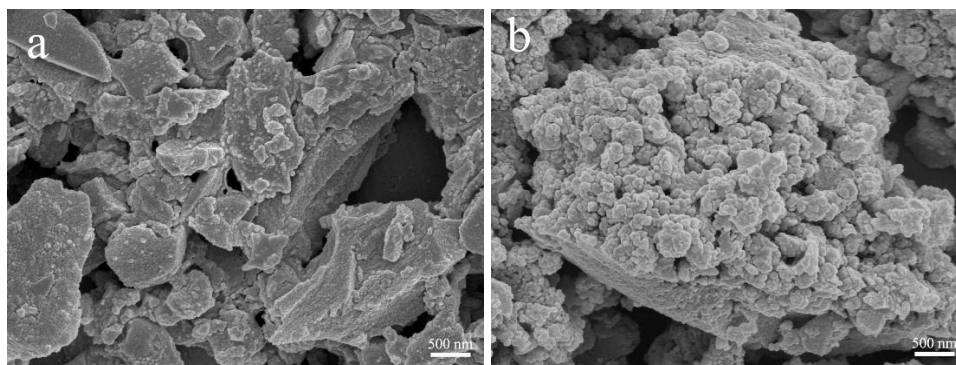

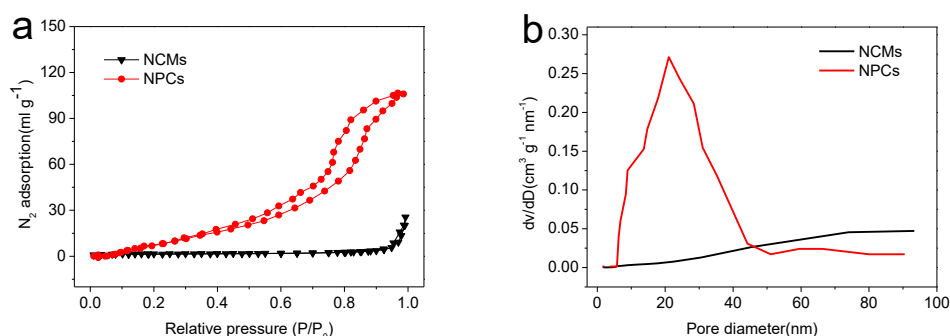**Figure 1.** SEM images of the samples; (a) NCMs;(b) c) NPCs

Figure 2. (a) N_2 adsorption-desorption isotherms of NCMs and NPCs and (b) the pore size distribution curves of NCMs and NPCs.

The nitrogen adsorption-desorption experiments of NPCs and NCMs were carried out to understand their surface and pore structure (Figure 2a). NPCs exhibit type-IV isotherms with a H3 hysteresis loops in the relative pressure range of 0.4-1.0. While NCMs show a low nitrogen adsorption capacity in relative pressure at 1.0. The NPCs hysteresis loop shows that it has mesopores with a wide pore size distribution. As shown in Figure 2a, the BET surface areas of NPCs is 68.2 m^2 g^{-1}, which is higher than that of NCMs (2.6m^2 g^{-1}). The pore size distribution curve indicates that the pores of NPCs are mainly distributed between 8 and 60 nm (Figure 2b). In addition, the total pore volumes of NCMs and NPCs are 0.01 and 0.33 cm^3 g^{-1}, respectively. This mesopores structure of NPCs inhibits the volumetric effect of the lithium insertion/extraction reaction, which can effectively reduce the migration distance of lithium ions [28]. When compare with NCMs, the larger surface are of NPCs can increase the contact area with the electrolyte, thus improving its electrochemical performance.
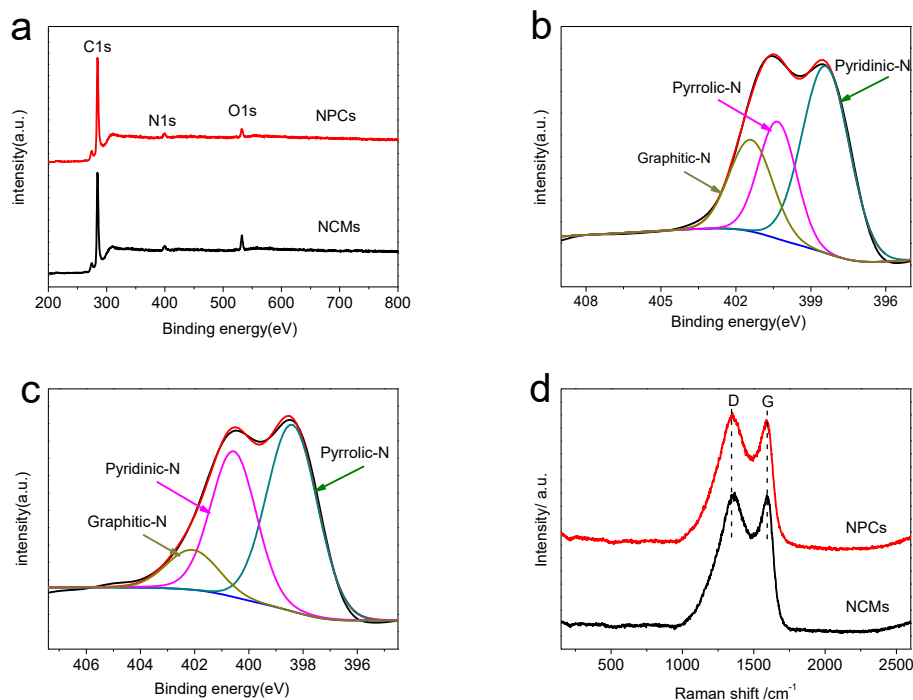
Figure 3. (a) The total XPS spectrum of the NPCs and NCMs, (b) curve fitting of N 1s spectra of the NCMs, (c) curve fitting of N 1s spectra of the NPCs, (d) Raman spectrum of NCMs and NPCs

Table 1. Element analysis of sample.

sample	Total element (wt%)			N 1s(wt%)		
	C	N	O	pyridinic N	pyrrolic N	graphitic N
NCMs	90.49	3.12	6.39	51.42	25.56	23.02
NPCs	92.10	3.80	4.10	51.27	37.60	11.13

In order to understand the influence of the nitrogen-doped type on the NCMs and NPCs, their elemental compositions were analyzed by XPS. The total spectrum of NCMs and NPCs, shown in Figure 3a, indicates the surface of NCMs and NPCs are composed of C, N, and O elements. As shown in Figure 3b and 3c, the N 1s spectra of NCMs and NPCs can be deconvoluted into three peaks at 398.4, 400.5, and 402.0 eV, indicating the existence of three types of nitrogen: pyridinic N (N-6), pyrrolic N (N-5) and graphitic N (N-Q) [29]. The pyridinic N replaces a carbon atom in a six membered ring. The pyrrolic N is located at a five membered ring and provides two electrons to the π-system of five membered ring. The graphitic N is nitrogen atom at graphite layer and bonded with three sp^2 carbon atoms. The element analysis is summarized in Table 1 and it is found that the major nitrogen types presented in NCMs and NPCs are pyridine N and pyrrolic N. It is worth mentioning that NPCs have a lower graphitic N content than NCMs. This is because NPCs has greater specific surface area and defects, and nitrogen atoms are more likely to located at the edge of graphite layer and NPCs defects [30, 31]. Previous researches indicate that, compared with graphitic N, pyridinic N and pyrrolic

N can not only provide more active sites in the process of lithium insertion/extraction reaction, but also increase the reversible capacity of LIBs [32].

The Raman spectra of NCMs and NPCs are shown in Figure 3d. For both samples, the D band appearing at 1365 cm^{-1} represents the disordered graphite or defective structure, the G band appearing at 1580 cm^{-1} represents the ordered graphite structure with sp^2 carbon [23, 33]. In addition, the I_D/I_G value reflects the degree of graphitization of the sample. The I_D/I_G value of NPCs (1.027) is higher than NCMs (0.991), indicates that NPCs has more defects and lower order structure [34]. Previous studies have reported that a high I_D/I_G value indicate that the nitrogen-doped atoms are mainly concentrated in the edge of graphite layer or in the defect (especially pyridinic N and pyrrolic N) [31].
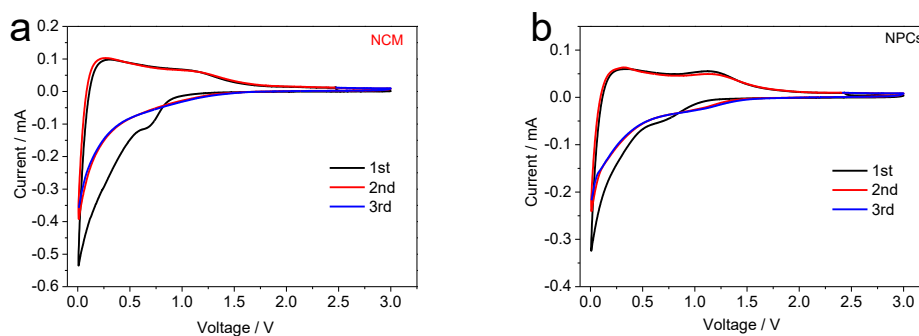

Figure 4. The CV curves of (a) NCM, (b)NPCs at a scan rate of 0.1 mV s^{-1} in the voltage window of 0.005V-3V
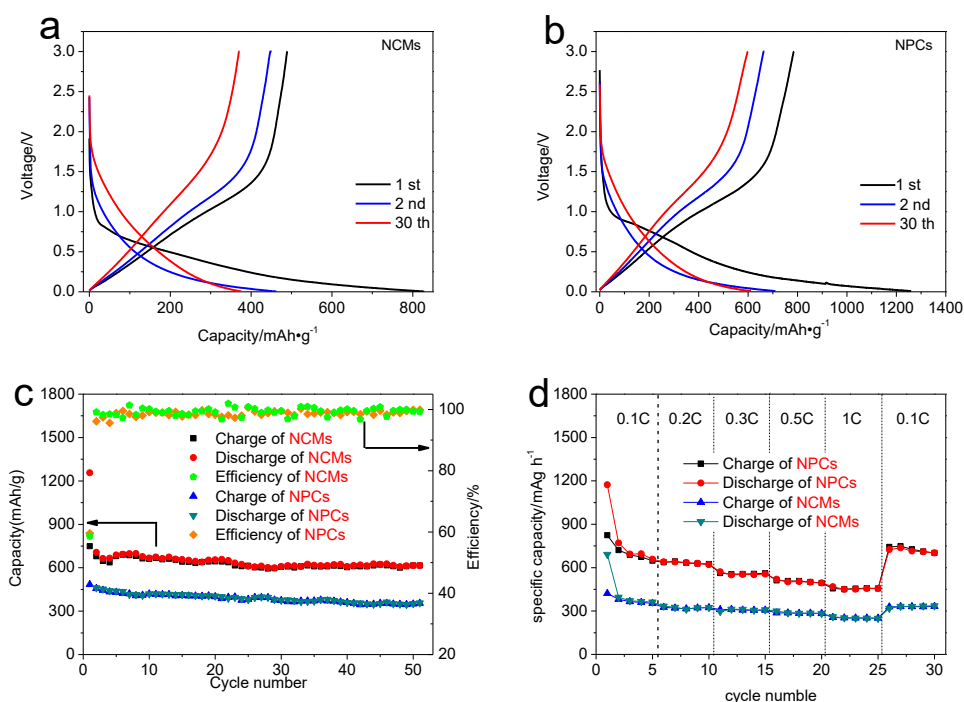

Figure 5. discharge-charge curves of (a) NCMs and (b) NPCs in tne first 3 cycles at 0.1 C, (c) cycle performance of NCMs and NPCs at 0.1C for 50 cycle, (d) rate performances of NCMs and NPCs at 0.1C-1C

The CV curves of NCMs and NPCs during the first 3 cycles, shown in Figure 4, exhibit typical CV curves of carbon materials. At the first cycle, the peak at 0.8 V in Figure 4a and 4b indicates the formation of SEI films [1, 35]. For all three cycles, the strong and sharp peaks at 0 V are caused by the intercalation of Li^+ into the carbon anode [36]. In addition, compared with NCMs, the NPCs exhibit new peaks at 1.2 V in the CV curves of NPCs, which is attributed to the extraction of Li^+ ion from the vacancies and the edges of the graphite layer [32]. This is consistent with the analysis of XPS.

Figures 5a and 5b present the discharge-charge profiles of NCMs and NPCs, respectively, at 0.1C. The initial discharge capacities of NCMs and NPCs are 826 mAh g^{-1} and 1256 mAh g^{-1}, respectively. And their initial charge capacities are 461 mAh g^{-1} and 748 mAh g^{-1}, respectively. The main reason for the capacity loss is the formation of SEI films on the surface of NCMs and NPCs, which agrees with the results of CV curves (Figure 4). Furthermore, the discharge-charge profiles of NCMs and NPCs at the first cycle has no apparent platform, which is due to the presence of amorphous carbon [3]. The cycle and rate performances of NCMs and NPCs are shown in Figures 5c and 5d, respectively. In the first cycle, the initial Coulombic efficiencies of NCMs and NPCs are 58.59% and 59.60%, respectively. Compared to NPCs, the lower initial discharge capacity and reversible capacity of NCMs may be attributed to its lower specific surface and higher contents of graphitic N [23]. The rate performances of NPCs are 648, 624, 561, 493, and 456 mAh g^{-1} at 0.1, 0.2, 0.3, 0.5, and 1 C, respectively, which are higher than the rate performance of NCMs (353, 323, 306, 283, and 250 mAh g^{-1} at 0.1, 0.2, 0.3, 0.5, and 1C, respectively).
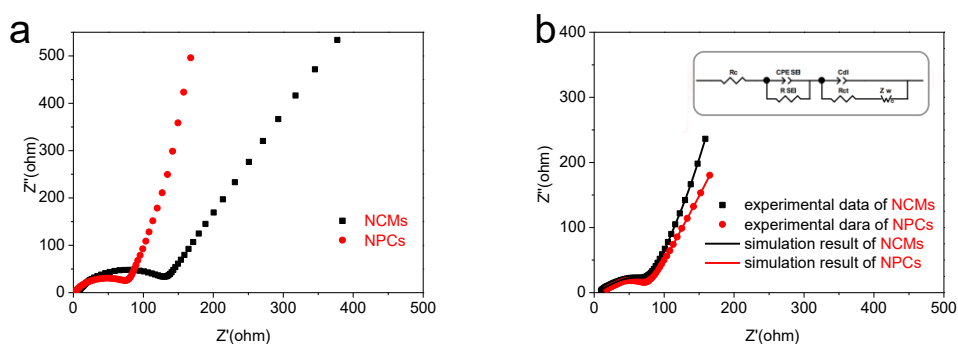

Figure 6. (a) EIS of NCMs and NPCs before CV, (b) EIS of NCMs and NPCs after CV (inset: equivalent circuit)

The EIS is used to explore the dynamics behavior of NCMs and NPCs for LIBs. The EIS of NCMs and NPCs before CV and after CV are shown in Figures 6a and 6b, respectively. As shown in Figure 6a, the semicircle diameter of NPCs is less than that of NCMs. The main reason is that NPCs has a reasonable pore structure, which can effectively shorten the migration distance of Li^+ ion, thus leading to a smaller charge-transfer resistance. This small charge transfer resistance is beneficial to the enhancement of NPCs capacity [37]. Furthermore, in order to investigate the effects of pore structure and nitrogen doping on the cyclic stability, EIS measurement were carried out on the NCMs and NPCs after CV finishing. According to the fitting circuit, the EIS of NCMs and NPCs were fitted by software Zview (Figure 6b inset). The fitting circuit contains resistance Rc, constant phase angle element

CPE$_{SEI}$, resistance R$_{SEI}$, constant phase angle element C$_{dl}$, resistance R$_{ct}$ and Warburing impedance Z$_w$ [38, 39]. The R$_{SEI}$ value of NPCs is 65.79 Ω, which is obviously lower than R$_{SEI}$ of NCMs (79.33 Ω). It implies that NPCs has a loose and stable SEI film, which is beneficial to the improvement of cyclic stability. Meanwhile, NPCs has a large contact area with electrolyte, and both pyridine N and pyrrole N in NPCs are favorable for forming stable SEI film on the surface of NPCs [40, 41]. The results indicate that total electric resistance of NPCs is decreased with increasing contents of pyridine N and pyrrole N. It is for this reason that the high electronic conductivity of the NPCs and the efficient contact between electrochemical active particles.

4. CONCLUSION

NPCs with high contents of pyrrolic N and pyridine N was synthesized by using a self-sacrifice template method with PS as template and PAN as carbon precursor. Compared with NCMs, the NPCs have higher specific surface area and lower graphitic N content. The high specific surface area and pores structure of NPCs shorten the migration distance of Li$^+$ and effectively increase the contact area with the electrolyte. Moreover, the high pyridinic N and pyrrolic N contents of NPCs increases the specific capacity by introducing more defects and vacancies in graphitic layers, and also improves its cycle stability by forming stable SEI films. Therefore, N-PCs exhibits much better electrochemical performance as anode materials of LIBs.

CONFLICTS OF INTEREST STATEMENT
The authors certify that they have NO affiliations with or involvement in any organization or entity with any financial interest (such as honoraria; educational grants; participation in speakers' bureaus; membership, employment, consultancies, stock ownership, or other equity interest; and expert testimony or patent-licensing arrangements), or non-financial interest (such as personal or professional relationships, affiliations, knowledge or beliefs) in the subject matter or materials discussed in this manuscript.

References

1. L. Qie, W. M. Chen, Z. H. Wang, Q. G. Shao, X. Li, L. X. Yuan, X. L. Hu, W. X. Zhang, Y. H. Huang, *Adv Mater*, 24 (2012) 2047.
2. S. Q. Zhang, R. Lin, W. B. Yue, F. Z. Niu, J. Ma, X. J. Yang, *Chemical Engineering Journal*, 314 (2017) 19.
3. F. Zhang, K. X. Wang, G. D. Li, J. S. Chen, *Electrochemistry Communications*, 11 (2009) 130.
4. Y. Zhong, X. Xia, F. Shi, J. Zhan, J. Tu, H. J. Fan, *Advanced science*, 3 (2016) 1500286.

5. P. Ramakrishnan, S.-H. Baek, Y. Park, J. H. Kim, *Carbon*, 115 (2017) 249.
6. F. Rohman, S. M. Nikmah, J. Triwibowo, *Journal of Physics: Conference Series*, 817 (2017) 012005.
7. D. Miranda, C. M. Costa, S. Lanceros-Mendez, *Journal of Electroanalytical Chemistry*, 739 (2015) 97.
8. J. Zhu, C. Chen, Y. Lu, Y. Ge, H. Jiang, K. Fu, X. Zhang, *Carbon*, 94 (2015) 189.
9. S. Zou, X. Xu, Y. Zhu, C. Cao, *Microporous and Mesoporous Materials*, 251 (2017) 114.
10. J. Wu, L. Zuo, Y. Song, Y. Chen, R. Zhou, S. Chen, L. Wang, *Journal of Alloys and Compounds*, 656 (2016) 745.
11. J. Liu, S. Wang, Q. Sun, *Proceedings of the National Academy of Sciences of the United States of America*, 114 (2017) 651.
12. A. D. Roberts, X. Li, H. Zhang, *Chem Soc Rev*, 43 (2014) 4341.
13. Y. Gao, J. Li, Y. Liu, L. Zhong, C. Shu, B. Yue, W. Zhang, *Ionics*, 23 (2017) 2301.
14. J. Ou, L. Yang, Y. Zhang, L. Chen, Y. Guo, D. Xiao, *Chinese Journal of Chemistry*, 33 (2015) 1293.
15. Z. F. Yu, X. Z. Wang, Y. N. Hou, X. Pan, Z. B. Zhao, J. S. Qiu, *Carbon*, 117 (2017) 376.
16. C. Jiang, J. Wang, Z. Chen, Z. Yu, Z. Lin, Z. Zou, *Electrochimica Acta*, 245 (2017) 279.
17. C. Schneidermann, N. Jackel, S. Oswald, L. Giebeler, V. Presser, L. Borchardt, *ChemSusChem*, 10 (2017) 2416.
18. L. Miao, H. Duan, M. Liu, W. Lu, D. Zhu, T. Chen, L. Li, L. Gan, *Chemical Engineering Journal*, 317 (2017) 651.
19. H. Lu, R. Chen, Y. Hu, X. Wang, Y. Wang, L. Ma, G. Zhu, T. Chen, Z. Tie, Z. Jin *et al*, *Nanoscale*, 9 (2017) 1972.
20. J. Zhao, H. Lai, Z. Lyu, Y. Jiang, K. Xie, X. Wang, Q. Wu, L. Yang, Z. Jin, Y. Ma *et al*, *Adv Mater*, 27 (2015) 3541.
21. J. Gong, H. Lin, M. Antonietti, J. Yuan, *J Mater Chem A*, 4 (2016) 7313.
22. P. Chen, L. K. Wang, G. Wang, M. R. Gao, J. Ge, W. J. Yuan, Y. H. Shen, A. J. Xie, S. H. Yu, *Energy & Environmental Science*, 7 (2014) 4095.
23. X. Wang, Q. Weng, X. Liu, X. Wang, D. M. Tang, W. Tian, C. Zhang, W. Yi, D. Liu, Y. Bando *et al*, *Nano letters*, 14 (2014) 1164.
24. L. L. Tian, S. B. Li, M. J. Zhang, S. K. Li, L. P. Lin, J. X. Zheng, Q. C. Zhuang, K. Amine, F. Pan, *ACS applied materials & interfaces*, 8 (2016) 26722.
25. Y. Yang, S. Jin, Z. Zhang, Z. Du, H. Liu, J. Yang, H. Xu, H. Ji, *ACS applied materials & interfaces*, 9 (2017) 14180.
26. D. Guo, R. Shibuya, C. Akiba, S. Saji, T. Kondo, J. Nakamura, *Science*, 351 (2016) 361.
27. E. Jo, J.-G. Yeo, D. K. Kim, J. S. Oh, C. K. Hong, *Polymer International*, 63 (2014) 1471.
28. D. C. Guo, F. Han, A. H. Lu, *Chemistry*, 21 (2015) 1520.
29. J. Zhou, L. Bao, S. J. Wu, W. Yang, H. Wang, *Journal of Materials Research*, 32 (2017) 404.
30. Y. Mao, H. Duan, B. Xu, L. Zhang, Y. Hu, C. Zhao, Z. Wang, L. Chen, Y. Yang, *Energy & Environmental Science*, 5 (2012) 7950.
31. F. Zheng, Y. Yang, Q. Chen, *Nature communications*, 5 (2014) 5261.
32. H. G. Wang, C. P. Yuan, R. Zhou, Q. Duan, Y. H. Li, *Chemical Engineering Journal*, 316 (2017) 1004.
33. J. Gong, H. Lin, K. Grygiel, J. Yuan, *Applied Materials Today*, 7 (2017) 159.
34. S. Gayathri, P. Jayabal, M. Kottaisamy, V. Ramakrishnan, *AIP Advances*, 4 (2014) 027116.
35. W. Wang, Y. Sun, B. Liu, S. Wang, M. Cao, *Carbon*, 91 (2015) 56.
36. T. Mei, L. Zhang, X. Wang, Y. Qian, *J Mater Chem A*, 2 (2014) 11974.
37. P. Liu, Q. Hao, X. Xia, L. Lu, W. Lei, X. Wang, *The Journal of Physical Chemistry C*, 119 (2015) 8537.
38. S. Zhang, P. Shi, *Electrochimica Acta*, 49 (2004) 1475.

39. M. M. Kamisah, H. Siti Munirah, M. S. Mansor, *Ionics*, 13 (2007) 223.
40. Y. Han, L. Dong, J. Feng, D. Li, X. Li, S. Liu, *Electrochimica Acta*, 167 (2015) 246.
41. H. Wang, C. Zhang, Z. Liu, L. Wang, P. Han, H. Xu, K. Zhang, S. Dong, J. Yao, G. Cui, *Journal of Materials Chemistry*, 21 (2011) 5430.